Nanoscale

Accepted Manuscript

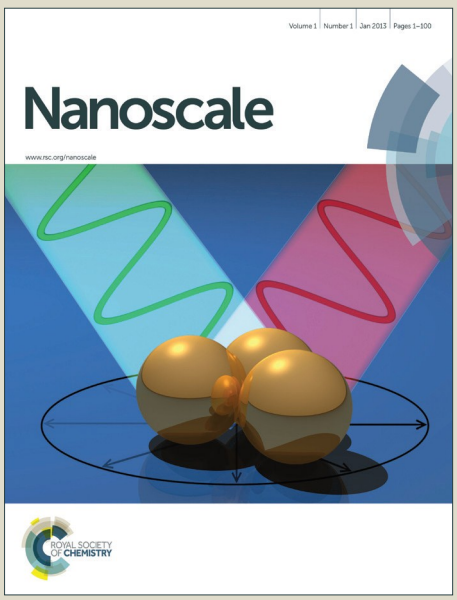

ROYAL SOCIETY OF CHEMISTRY

www.rsc.org/nanoscale

Strontium-incorporated Nanoporous Titanium Implant Surface for Rapid Osseointegration

Wenjie Zhang [a,1], Huiliang Cao [b,1], Xiaochen Zhang [a,1], Guanglong Li [a], Qing Chang [c], Jun Zhao [a], Yuqin Qiao [b], Xun Ding [a], Guangzheng Yang [a], Xuanyong Liu [b,**], and Xinquan Jiang [a,*]

[a] Department of Prosthodontics, Oral Bioengineering and regenerative medicine Lab, Ninth People's Hospital Affiliated to Shanghai Jiao Tong University, School of Medicine, 639 Zhizaoju Road, Shanghai 200011, China

[b] State Key Laboratory of High Performance Ceramics and Superfine Microstructure, Shanghai Institute of Ceramics, Chinese Academy of Sciences, 1295 Ding-xi Road, Shanghai 200050, China

[c] Shanghai Institute of Digestive Surgery and Department of Surgery, Rui Jin Hospital, Shanghai Jiao Tong University, School of Medicine, 197 Ruijin Road II, Shanghai 200025, China

[1] These authors contributed equally

* Corresponding author. Department of Prosthodontics, College of Stomatology, Ninth People's Hospital, School of Medicine, Shanghai Jiao Tong University, 639 Zhizaoju Road, Shanghai 200011, PR China.

** Corresponding author. State Key Laboratory of High Performance Ceramics and Superfine Microstructure, Shanghai Institute of Ceramics, Chinese Academy of Sciences, Shanghai 200050, PR China. Tel./fax: +86 21 52412409.

E-mail addresses: xinquanjiang@aliyun.com (X. Jiang), xyliu@mail.sic.ac.cn (X. Liu).

KEYWORDS: micro-arc oxidation; nano-scale pores; strontium ion; dental implant; osseointegration; angiogenesis.

ABSTRACT

Rapid osseointegration of dental implants will shorten the period of treatment and enhance the comfort of patients. As the vital role of the angiogenesis played during bone development and regeneration, it is might be feasible to promote rapid osseointegration by modifying the implant surface to gain a combined angiogenesis/osteogenesis inducing capacity. In this study, a novel coating (MAO-Sr) with strontium-incorporated nanoporous structures on titanium implants was generated via a new micro-arc oxidation, in an attempt to induce angiogenesis and osteogenesis to enhance the rapid osseointegration. *In vitro*, the nanoporous structure significantly enhanced the initial adhesion of canine BMSCs. More importantly, sustained release of strontium ions also displayed a stronger effect on the BMSCs in facilitating their osteogenic differentiation and promoting the angiogenic growth factors secretion to recruit endothelial cells and promote blood vessels formation. Advanced mechanism analyses indicated that MAPK/Erk and PI3K/Akt signaling pathways were involved in these effects of the MAO-Sr coating. Finally, in the canine dental implantation study, the MAO-Sr coating enhanced faster bone formation within initial six weeks and the osseointegration effect was comparable to that of the commercially available ITI implants. These results suggest that the MAO-Sr coating has the potential for future use in dental implants.

Introduction

About fifty years ago [1], professor Brånemark first reported the phenomenon of osseointegration and introduced it into prosthetic dentistry field. Nowdays, dental implants has become a widely popular method for replacing missing teeth. However, according to the guideline of classical implant dentistry, the patient needs to wait at least 3 months to acquire adequate osseo-integrated fixation after implants installation before prosthetic procedure and loading [2]. In order to shorten the healing period and improve esthetic and masticating functions, various modifications on titanium implants surface have been applied to enhance the rapid osseointegration by promoting osteogenic differentiation [3]. Actually, more and more evidences indicate that angiogenesis process in bone and osteogenesis are coupled [4-7]. Blood vessels play an important role in promoting bone healing because that they are not only transport essential oxygen and nutrients, but also can deliver osteogenic cells and even secrete osteoinductive growth factors to the region of bone defect [6-8]. It has been well documented that the application of vascularization strategies in tissue engineering can obviously enhance bone regeneration [9-12]. Histological observation indicated that blood vessels are concentrated within the implant surface concavities [13]. And the angiogenesis process around dental implants also can facilitate local bone regeneration and increase the degree of osseointegration [14, 15]. Therefore, we propose here a concept that the combined angiogenic/osteogenic-inducing ability of dental implant surface for enhancing rapid osseointegration.

In general, surface treatments of titanium dental implants can be divided into three broad categories: surface topography [16, 17], chemical composition [18, 19] and drug delivery [20, 21]. Surface structures, including micro-, nano- and micro-/nano- scales, have been demonstrated to direct protein adsorption, cell adhesion, osteogenic differentiation and thus the rate and quality of osseointegration [3, 22-24]. In addition, some surface profiles have been reported to enhance angiogenesis by upregulating the expression of angiogenic growth factors [25, 26]. The chemical compositions of implant surface also play an important role in the adsorption of proteins and adhesion of osteoblastic cells. Especially, the incorporation of many bioactive ions (e.g. Ca, Si, Zn,

Sr and Mg) can significantly induce the osteogenic differentiation of stem cells [18, 27]. Meantime, some of these ions, like strontium, can enhance angiogenesis both *in vitro* and *in vivo* [28-30]. For drug delivery, recombination proteins have been used to enhance angiogenesis and bone regeneration around titanium implants [31, 32]. And suitable surface structures can facilitate drugs loading and improve the release efficiency [33, 34]. Taking together, a new implant surface possessing all of these advantages might be more suitable for promoting both of angiogenesis and osteogenesis, and then rapid osseointegration.

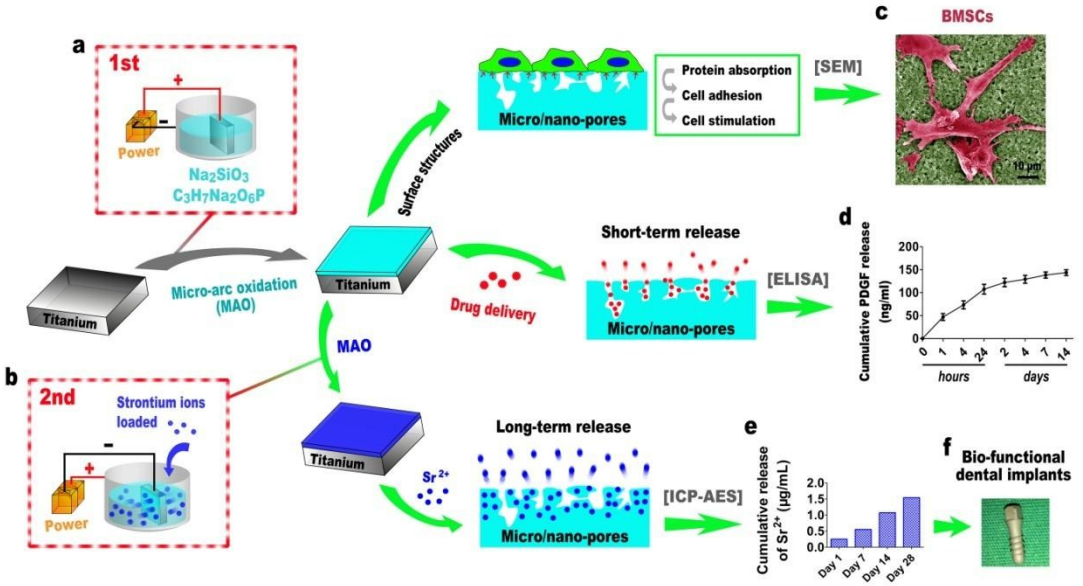

Fig. 1. Schematic of the fabrication protocols for the novel strontium incorporated micro-arc oxidation (MAO) coatings with multifunctions. (a) The first MAO for generating micro/nano-pores modified coating. (b) The second MAO for incorporating strontium ions. (c) SEM image shows canine BMSCs (red color) adhesion on the micro/nano-scale structures. (d) Cumulative release curve of PDGF proteins from the nano-pores on the MAO coatings, detected by the ELISA assay. (e) Cumulative release of strontium ions from the MAO-Sr coatings, detected by the ICP-AES assay. (f) The photo of the MAO-Sr coated dental implant, which was implanted in the canine mandible in this study.

In the present study, we fabricated a multi-functional titanium surface using a new micro-arc oxidation (MAO) technique with a high-conductivity solution and low

operating voltage (Fig. 1a). The novel TiO_2 layer (MAO group) displayed uniform hierarchical micro/nano-topography and homogeneously distributed nano-scale pores, unlike those different sized micro-scale holes generated by traditional MAO technique. The biological properties of the micro/nano-topography were evaluated by tests on the proliferation, adhesion and angiogenic/osteogenic differentiation of canine bone marrow stem cells (BMSCs). In addition, we also tested the drug delivery ability of these nano-pores system for recombinant human platelet derived growth factor-BB (rhPDGF-BB) release to induce angiogenic/osteogenic differentiation of BMSCs. Furthermore, we developed an innovative secondary MAO technique to incorporate strontium into the new titanium surface (Fig. 1b). And the efficacy and the underlying mechanisms, by which such a bioactive titanium surface (MAO-Sr group) promotes rapid osseointegration, were investigated with *in vitro* and even *in vivo* canine mandible implantation models.

Materials and methods

Animals

The canines used in this study were obtained from the Ninth People's Hospital Animal Center (Shanghai, China) and the experimental protocol was approved by the Animal Care and Experiment Committee of the Ninth People's Hospital.

Fabrication and characterization of MAO-Sr coating

Commercial TC4 titanium alloy was cut into squares (10×10×1mm or 20×20×1mm for in vitro studies) or machined into dental implants (for in vivo studies). The samples were ultrasonically cleaned in acetone, acid pickled, and ultrasonically cleaned with ethanol. Then, the samples were micro-arc oxidized (MAO) in an electrolyte containing 4.5 g/L glycerophosphate disodium salt pentahydrate ($C_3H_7Na_2O_6P•5H_2O$, Kelong, Shanghai, China) and 4.0 g/L sodium metasilicate nonahydrate ($Na_2SiO_3•9H_2O$, Sinopharm, Shanghai, China) to fabricate a porous surface layer (the MAO coating). In order to load strontium into the porous

surface layer (the MAO-Sr coating), the samples, after micro-arc oxidization, were further electrochemical treated in a strontium dichloride solution ($SrCl_2$•$6H_2O$, Sinopharm, 10.0 g/L) by applying a negative potential (0.5 A/cm^2) on the samples (graphite as the counter electrode) for 30 min. The surface morphology of the samples was observed using a scanning electron microscopy (SEM, JEOL JSM-6700F, Japan) and the phase structures of the materials was determined by a X-ray diffractometry (Bruker D8 Discover, Germany). The elemental compositions and mappings (Ti and Sr) of the MAO-Sr coating were determined by energy-dispersive X-ray spectrometry (EDS, EPMA, JAX-8100, Japan). The chemical states of strontium (Sr) were determined by X-ray photoelectron spectroscopy (XPS) (Physical electronics PHI 5802). For the detection of strontium ions release, titanium implants with MAO-Sr coating were in 5 ml physiological saline (0.9% NaCl, pH 7.0) at 37 ℃ without stirring, and the extracts were collected and refreshed with fresh solution at day 1, 7, 14, and 28, and then the amounts of released strontium ions were determined by inductively-coupled plasma optical emission spectrometry (ICP-OES, Varian, USA). Scratching test was carried out to evaluate the adhesion strength of the coatings.

Delivery of rhPDGF-BB by the nanopores

GEM 21S® containing rhPDGF-BB was provided by BioMimetic Therapeutics, Inc., Franklin, TN, USA. Square titanium plates (10 mm in length) with MAO coating were used to test the ability on the loading of growth factors. According to our previously described procedures [20], a total of 50 μl rhPDGF-BB solution with a concentration of 100 μg/ml was added onto each titanium plate, and then the samples were taken for 10 min vacuum extraction before air-drying at 4 ℃ overnight. The release of rhPDGF-BB at selected time points was measured using an ELISA kit (BD Biosciences, San Jose, CA, USA) [20]. Canine BMSCs were isolated and cultured as we previously described [18]. The proliferation activity of these cells on the rhPDGF-BB loaded MAO surface was detected by MTT assay at day 1, 3, 5, and 7. For angiogenic and osteogenic differentiation assay, cells total RNA were extracted after 7 days incubation and measured using the Bio-Rad Quantitative Real time PCR system

(RT-PCR; Bio-Rad, MyiQ^{TM}, USA) (primers see Table S1, Supporting Information).

BMSCs adhesion on MAO-Sr coating

For cell adhesion detection, the expression of integrin β1 after initial seeding was measured. At the gene level, total RNA were collected at 4 and 12 hours, and then measured by the RT-PCR (primers see Table S1, Supporting Information). At the protein level, cells were fixed after 12 hours incubation and detected using the immunofluorescence method as we previously described [18]. Briefly, specific primary antibody targeting integrin β1 (Abcam, Cambridge, UK) and DyLight 549-conjugated anti-mouse IgG antibody were used to detect the expression of integrin β1 in the experiment. Cell cytoskeleton and nuclei were counterstained with FITC-Phalloidin (Enzo Life Science Ltd., Exeter, UK) and DAPI (Invitrogen, Carlsbad, CA, USA), respectively.

BMSCs osteogenic differentiation induced by MAO-Sr coating

After incubation in DMEM for 7 days, canine BMSCs were fixed and stained with ALP kit (Beyotime, Shanghai, China). Meantime, ALP quantitative assay was measured using the p-nitrophenyl phosphate (pNPP) (Sigma, St. Louis, MO, USA) according to our previously described procedures [18]. Calcium deposition assays were further performed after culture in DMEM for 14 days. Firstly, cells were stained with 40 mM Alizarin Red S (ARS, Sigma) solution after fixing in 70% ethanol. And then, the stained wells were eluted using a solution of 10% cetylpyridinium chloride (Sigma) and the OD values were measured at 590 nm for quantitative assay [18]. The expression of RUNX 2 , ALP, OPN, and OCN were further detected using the immunofluorescence method after incubation in DMEM for 7 days.

Angiogenic effects of the MAO-Sr coating

Canine BMSCs incubating on the MAO-Sr coating, the release of angiogenesis related growth factors, VEGF and PDGF-BB, were measured using the ELISA method by collecting the culture medium at day 1, 3, 5, and 7. In addition, we further

detected the angiogenic effects of these secreted growth factors on the *in vitro* recruitment and *in vitro* angiogenesis abilities of endothelial cells. The culture medium were collected and added in the lower chambers of the transwell plates with 8 μm pore membranes to test the recruitment capacity on HUVECs (AllCells, Shanghai, China), which were incubated in the upper chambers [11]. After 24 hours culture, these cells penetrated the membranes of the upper chambers were fixed and observed under a microscope. The *in vitro* endothelial tube formation assay was tested on the ECMatrix™ gel (Millipore, Billerica, MA, USA) according to the manufacturer's instructions. In this experiment, endothelial cell growth medium (AllCells) was used to collect the secreted growth factors, and then was taken for HUVECS culture for 24 hours to form cellular network structures.

Molecular mechanism detection

Canine BMSCs were incubated on the titanium plates with different coatings in 6-well plates for 12 hours. Total cell protein was harvested using a protein extraction regent (Kangchen, Shanghai, China) with phosphatase inhibitor cocktail. Western blot analysis was taken to observe the activation of MAPK/Erk and PI3K/Akt signaling pathways by testing the expression of Erk1/2, p-Erk1/2, AKT, and p-AKT. In addition, the released ions were collected and tested on the activation of these two signaling pathways. Canine BMSCs were incubated in the extracts from different coatings for 12 hours before taking for western blot assay. More experiments were further designed to test whether the activation of these two signaling pathways are involved in the angiogenic/osteogenic effects of the MAO-Sr coating. Canine BMSCs were incubated on the MAO-Sr coating in the culture medium containing Erk1/2 signaling pathway inhibitor PD98059 (CST, Beverly, MA, USA) or/and Akt signaling pathway inhibitor LY294002 (CST) with a final concentration of 10 μM. After 3 days culture, cell total RNA was isolated and used for RT-PCR detection on the expression of VEGF, PDGF-BB, ALP, and OCN (primers see Table S1, Supporting Information).

In vivo animal study

Totally twelve adult beagle dogs, about 18 months old, were used for *in vivo* mandible dental implantation study. Under general anesthesia, all premolars and first molar of the left mandible of six dogs were extracted and left for 3 months for tooth extraction wound healing. At the edentulous area, three implant holes were drilled and randomly inserted with the following dental implants, MAO, MAO-Sr and ITI. Two kinds of fluorochromes were administered intraperitoneally at a sequence of 30 mg/kg Alizarin Red S and 20 mg/kg Calcein (CA, Sigma) at 2 and 4 weeks after the surgery, respectively. Six weeks later, all animals were sacrificed and the left mandibles with three implants were harvested. And then, the specimens were fixed, dehydrated, embedded in polymethylmetacrylate (PMMA) and sectioned using a Leica SP1600 saw microtome (Leica, Hamburg, Germany). Finally, the sections were taken for fluorescence labeling observation before being staining with Von Gieson's picro fuchsin for new bone formation and osseointegration observation. Another six beagle dogs were used for rapid osseointegration evaluation on the femur implantation model, according to our previously reported procedures [18].

Statistical analysis

The data were presented as mean ± standard deviation (SD). Statistical analysis was performed with One-way ANOVA followed by Tukey's post hoc test using a SAS 8.2 statistical software package. Values of $p < 0.05$ and $p < 0.01$ were considered to be statistically significant.

Results and discussion

Fabrication and characterization of the nano-scale pores

New coatings (MAO and MAO-Sr groups) were fabricated on the acid-etched titanium surface (Ti group) and still displayed micrometer-sized pits (Fig. 2a, 1k×), and covered with uniform sub-micro-scale particles (Fig. 2a, 5k×). More importantly, high dense nano-scale (Ø, 50-500 nm) pores were found among these particles (Fig. 2b). From the cross-section (Fig. 2c), the thickness of the new coatings was about 1

μm, which is much less than that fabricated by traditional MAO technique (about 10 μm). There were abundant tunnels connected with the surface opening nano-scale pores in these new coatings, but no obvious gaps were found at the interface between the coatings and titanium basal body. And the adhesion strength of these coatings was as high as 30 N (Fig. S1, Supporting Information). Together, these micro-/nano-structures increased the surface area, which is favorable for drug delivery and element incorporation. We firstly tested the function of these nanopores for rhPDGF-BB delivery to promote angiogenesis and osteogenesis. Protein particles were loaded through vacuum method as we previously reported [20]. There was obvious release of rhPDGF-BB during the initial 24 hours, following a low level continuous release up to 14 days (Fig. 1d and Fig. S2a, Supporting Information). PDGF-BB is a potent mitogen and also well known for its angiogenic and osteogenic effects [20]. By loading rhPDGF-BB into nanopores, the new titanium surface not only promoted the proliferation of canine BMSCs (Fig. S2b, Supporting Information), but also enhanced the expression of angiogenic and osteogenic related genes (Fig. S2c, Supporting Information). Therefore, drug delivery is one of the major functions of these nanopores, to further promote rapid osseointegration and even to treat osteoporotic patients [20].

In the present study, strontium ions were added to the processed surface via a lower voltage for a short time, so these sub-micro-particles and nano-pores had not been destroyed (Fig. 2a,b). By linking the sample to the negative pole during secondary MAO, strontium ions quickly moved to the sample and were eventually incorporated into the surface. The quantity and the invasion depth of these immersed ions could be simply controlled through adjusting working voltage and processing time (data not shown). According to the energy-dispersive X-ray spectrometry (EDS) mappings (Fig. 2d), there were uniform distributions of Sr on the surface of MAO-Sr group sample. The X-ray diffraction (XRD) spectra of the materials (Fig. 3a) indicated that anatase and rutile forms of titanium dioxide were the major phases in the coatings of MAO and MAO-Sr groups (the α-Ti and β-Ti were from the titanium substrate). And the trace components in the MAO-Sr group were evidenced by

using the X-ray photoelectron spectroscopy (XPS) technique. As depicted in Fig. 3b, the Sr 3d doublets at 133.58 eV /135.29 eV and 132.74 eV /134.50 eV, with a separation of approximately 1.7eV, correspond to strontium carbonate ($SrCO_3$) and strontium titanate ($SrTiO_3$). Accordingly, the Sr-loading process can be expressed as: Firstly, strontium dichloride was dissolved to produce strontium ions

$$SrCl_2 \rightarrow Sr^{2+} + 2Cl^- \quad (1)$$

The resulted strontium ions were driven toward the sample surface by the electric field. And some of them were inserted into the titanium dioxide lattices to produce strontium titanate ($SrTiO_3$), the others were reduced to become metallic strontium

$$Sr^{2+} + 2e \rightarrow \mathrm{Sr} \quad (2)$$

The metallic strontium was further oxidized due to expose to atmosphere, and transferred into strontium carbonate ($SrCO_3$).

Additionally, the incorporated strontium ions were continuously released at a relatively high level within 28 days and without initial robust release (Fig. 1e), which might maintain the long term bioactive effects. The new surface fabrication technique is also suitable for three dimensions implants and has the advantages of simple operation, good repeatability and low cost. The bio-functional dental implants (MAO-Sr coated surface, Fig. 1f) were fabricated and could be easily preserved and shipped, raising the likelihood for potential future clinical applications.

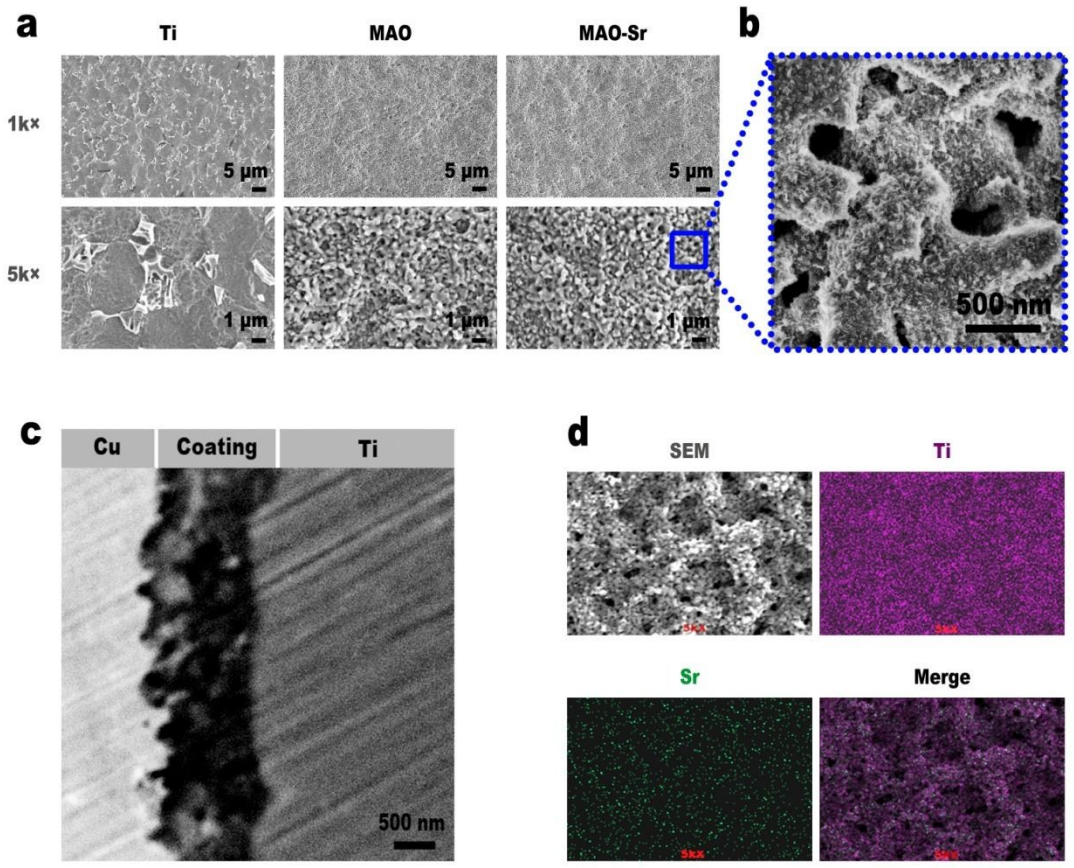

Fig. 2. Surface and cross-sectional microstructures of the coatings. (a) Surface microstructures of the titanium before and after MAO (or MAO-Sr) treatment. (b) Typical surface nano-pores structures of the MAO-Sr coating in high magnification. (c) Typical cross-sectional microstructure of the MAO-Sr coating. (d) Energy-dispersive X-ray mapping of titanium (Ti) and strontium (Sr) on MAO-Sr coating.

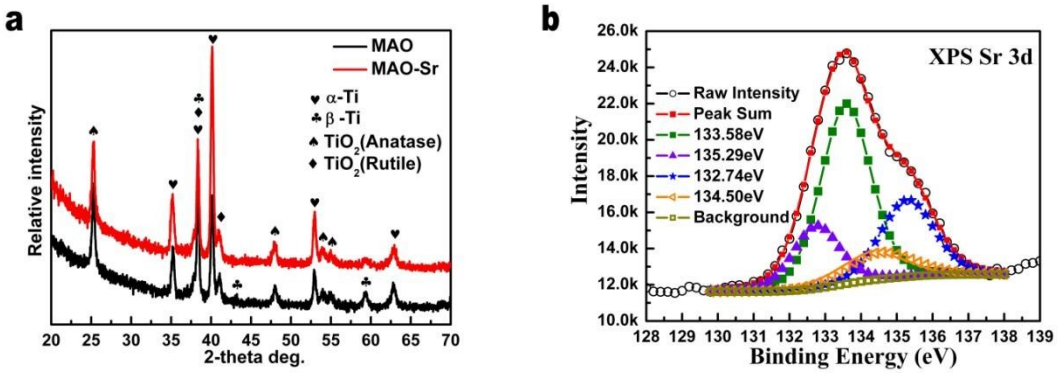

Fig. 3. (a) X-ray diffraction patterns acquired from the coatings. (b) XPS Sr 3d spectra of the MAO-Sr group.

Nano-scale pores promote cell adhesion

Canine BMSCs were cultured on different titanium plates *in vitro*, although there were no significant differences of cells metabolic activity among the three groups displayed by MTT results (Fig. 4a), nano-scale pores obviously enhanced cell adhesion. According to the quantitative real-time PCR (RT-PCR) results, the expression levels of adhesion related gene integrin β1 at two early time points (4 and 12 hours) in group MAO and group MAO-Sr were significantly higher than that in group Ti, while no significant differences were detected between the two groups of coatings covered with nanopores (Fig. 4b). Cell immunofluorescence staining of integrin β1 was further taken to confirm above findings at the protein level (Fig. 4c). At 24 h of culture, red fluorescence stained integrin β1 in group Ti was less abundant than that for the other two groups with nanoporous structure, and these results were consistent with that at gene level. As far as we know, the nano-scale pores promoted BMSCs adhesion might occur through facilitating serum proteins absorption [20, 35]. Good cell adhesion activity, especially the up-regulation of integrin β1, plays an important role in stimulating Integrin/FAK signaling pathways, which can further activate many downstream pathways, such as MAPK/Erk and PI3K/Akt, having close relationship with both of angiogenic and osteogenic differentiation [36-38].

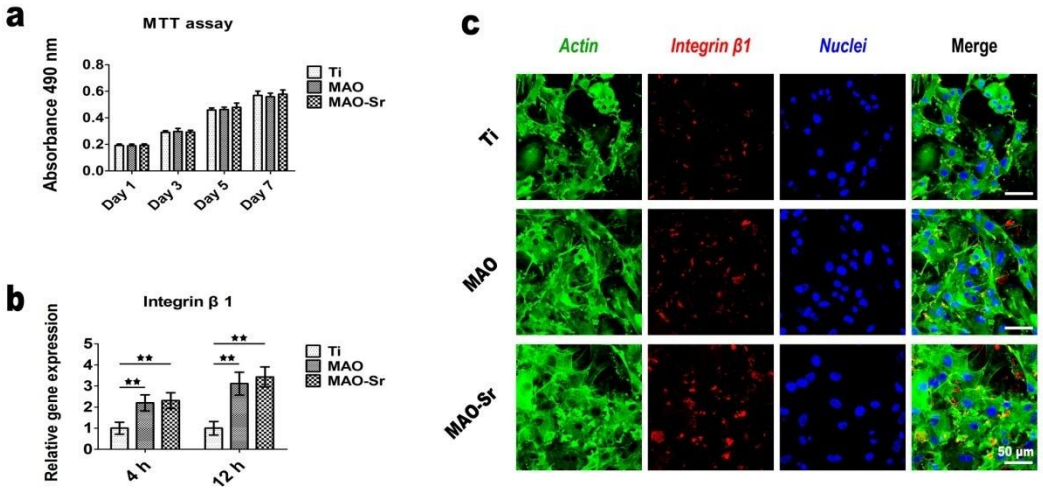

Fig. 4. The proliferation and adhesion activities on the new titanium coatings. (a) Canine BMSCs were cultured on the titanium plates for 1, 3, 5, and 7 days, and detected by MTT assay. Error bars

represent SD (n=4). (b) RT-PCR detection of integrin β1 gene expression in canine BMSCs after incubating on the titanium plates for 4 and 12 hours. Error bars represent SD (n=3). (c) The expression of integrin β1 at the protein level was detected by immunofluorescence assay after incubating on the titanium plates for 24 hours. "Merge" represents the merged images of actin (green), integrin β1 (red) and nuclei (blue). (★★, represents $p < 0.01$).

New coatings enhance in vitro angiogenic activity and osteogenic differentiation

As described above, the combined angiogenic/osteogenic ability might enhance *in vivo* fast oseeointegration. The effects of these new coatings (MAO and MAO-Sr) on the differentiation of canine BMSCs were evaluated by a wide array of experiments. For osteogenic differentiation, both of ALP activity and calcium deposition ability of MAO group were significantly enhanced when compared with Ti group, and these osteogenesis activities were further enhanced after strontium ions incorporation at MAO-Sr group (Fig. 5a-c). Moreover, after 14 days incubation in DMEM culture medium, there was obviously calcium deposition in MAO-Sr group, which definitely reflects the potent osteoinductive capacity of the new coating. According to the immunofluorescence staining results after 7 days culture (Fig. 5d,e), the expression of four major osteogenic markers (RUNX 2, ALP, OPN and OCN) were all higher in MAO group than those in the control group, and the highest expression of these markers were found in MAO-Sr group.

As for the angiogenic activity, the secretion of VEGF and PDGF-BB proteins were also enhanced in the MAO group, but were lower when compared to the MAO-Sr group according to the ELISA detection results (Fig. 5f,g). Both of VEGF and PDGF-BB are vital angiogenic regulators [39, 40], so the sustained secretion of those growth factors might promote angiogenesis activity around the implants. These secreted growth factors were further collected and tested on the recruitment and *in vitro* endothelial tube formation of human umbilical vein endothelial cells (HUVECs). As we expected, more and more HUVECs were recruited as the increase of these growth factors from group Ti to group MAO, and then to group MAO-Sr, and there were significant differences among the three groups (Fig. 5h,i). A similar tendency

was also observed in the *in vitro* tube formation experiment (Fig. 5h,j). We must explain here that the collected culture medium include released ions from the titanium coatings. Although we did not eliminate the effects of these ions in the two *in vitro* experiments on HUVECs, we still can speculate that the new coatings, when implanted *in vivo*, might promote initial angiogenesis mainly via stimulating attached cells to secrete angiogenic growth factors to recruit and facilitate endothelial cells to form blood vessels.

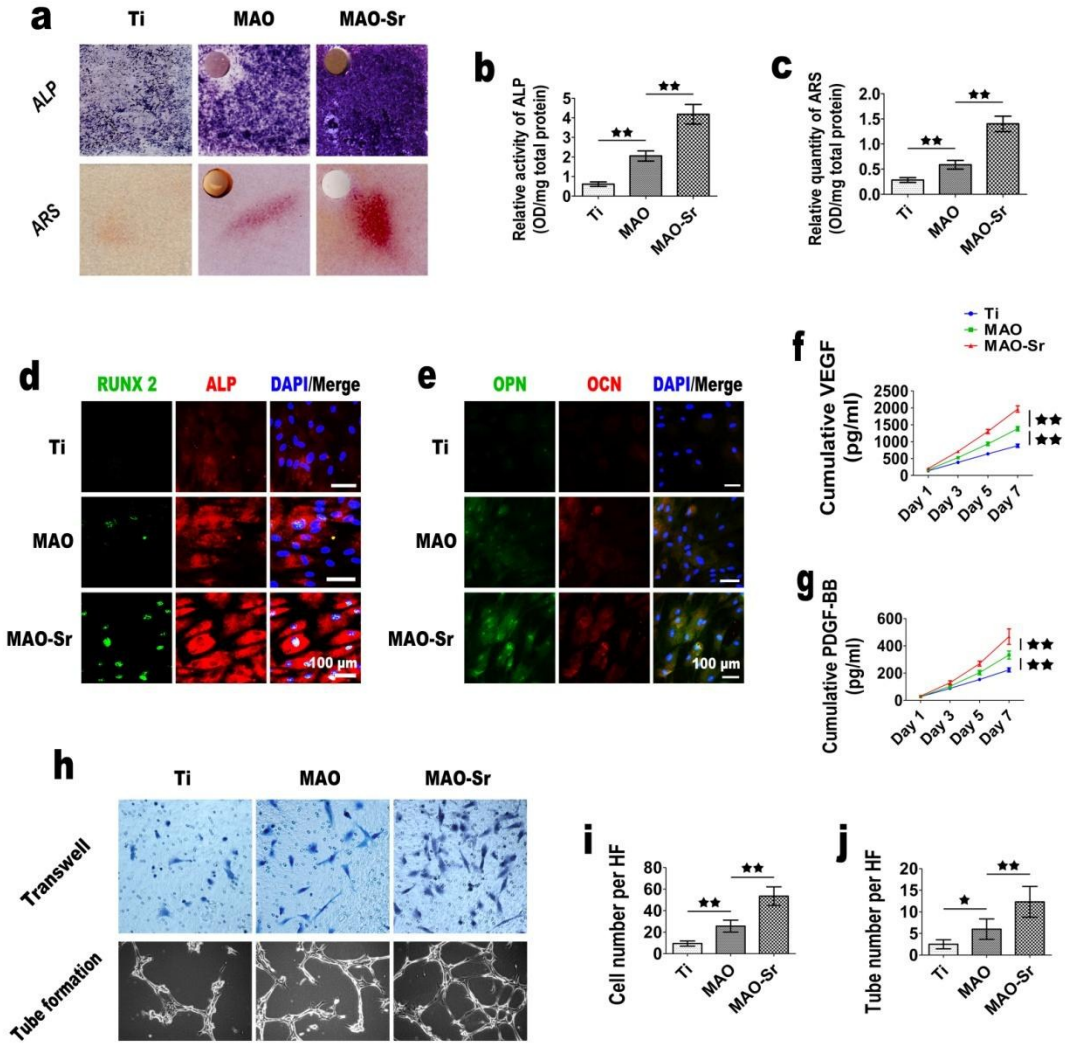

Fig. 5. The angiogenic and osteogenic effects of the new coatings on canine BMSCs. (a) ALP staining and alizarin red s (ARS) staining were performed after incubating the BMSCs on titanium plates for 7 days and 14 days, respectively. (b) Quantitative analysis of ALP activity of the BMSCs after 7 days culture. Error bars represent SD (n=4). (c) Quantitative assay of the calcium deposition capacity of the BMSCs after 14 days culture. Error bars represent SD (n=4). (d) The

expressions of RUNX 2 and ALP in BMSCs were simultaneously detected by immunofluorescence assay after 7 days culture. (e) The expression of OPN and OCN at the protein level in BMSCs after 7 days culture. (f-g) Canine BMSCs were incubated on titanium plates and the secretion of VEGF and PDGF-BB proteins into the culture medium at different times were detected by the ELISA assay. Error bars represent SD (n=6). (h) Images in the upper panels displayed the HUVECs penetrated the transwell membranes, under the induction of the collected BMSCs culture medium, containing VEGF and PDGF-BB proteins, for 24 hours. Images in the lower panels showed the *in vitro* tube formation of HUVECs incubated in the collected BMSCs culture medium for 24 hours. (i) The statistics of the numbers of these HUVECs penetrated the transwell membranes. Error bars represent SD (n=6). (j) The statistics of the numbers of the *in vitro* formed vessels. Error bars represent SD (n=6). (★, represents $p < 0.05$; ★★, represents $p < 0.01$).

Erk1/2 and Akt pathways involve in the angiogenic/osteogenic effects of the new coatings on canine BMSCs.

Experiments were further taken to examine the signaling mechanisms of the new coatings in promotion of angiogenic/osteogenic activities. MAPK/Erk1/2 and PI3K/Akt are known as two main signaling pathways that responsible for the inducing of both of angiogenic and osteogenic activities [41]. Activation of Erk1/2 can enhance the expression of hif-1α, which plays an important role in the coupling of angiogenesis and osteogenesis [42, 43]. And PI3K/Akt can work as the downstream signaling of hif-1α during the hypoxia-induced angiogenic and osteogenic responses [44]. In addition, PI3K/Akt has been reported as the main signaling pathway involved in PDGF-BB induced angiogenesis during coupling with osteogenesis [45]. In our study, western blot (WB) analysis showed that both of the two new coatings could induce phosphorylation of Erk1/2 and Akt signaling pathways, and the activation effects of MAO-Sr group were higher than that of MAO group (Fig. 6a, b). To distinguish the effect of surface structure and released ions on the activation of these two pathways, extracts from three samples were collected and tested on canine BMSCs. WB results indicated that extracts from MAO group mainly activate Akt pathway, but the two

tested pathways were all activated by extracts from MAO-Sr group (Fig. 6c, d). Based on above results, we might speculate that the surface structure was mainly involved in the Erk1/2 pathway, and the released ions, especially Sr^{2+}, activated both of Erk1/2 and Akt pathways.

Samples of MAO-Sr group were selected to identify whether the activation of Erk1/2 and Akt pathways is necessary for the angiogenic/osteogenic effects. Erk1/2 and Akt pathways were specifically inhibited by PD98059 and LY294002, respectively. RT-PCR results (Fig. 6e-h) showed that the new coating significantly enhanced the expression of angiogenic (VEGF and PDGF) and osteogenic (ALP and OCN) genes when compared with the control group (Ti group). More importantly, these advantages of MAO-Sr group were attenuated after the adding of single or both of the signaling inhibitors, but the genes expression in Ti group were not affected. The results confirmed that both of Erk1/2 and Akt pathways are involved in the angiogenic/osteogenic effects of MAO-Sr coating on canine BMSCs.

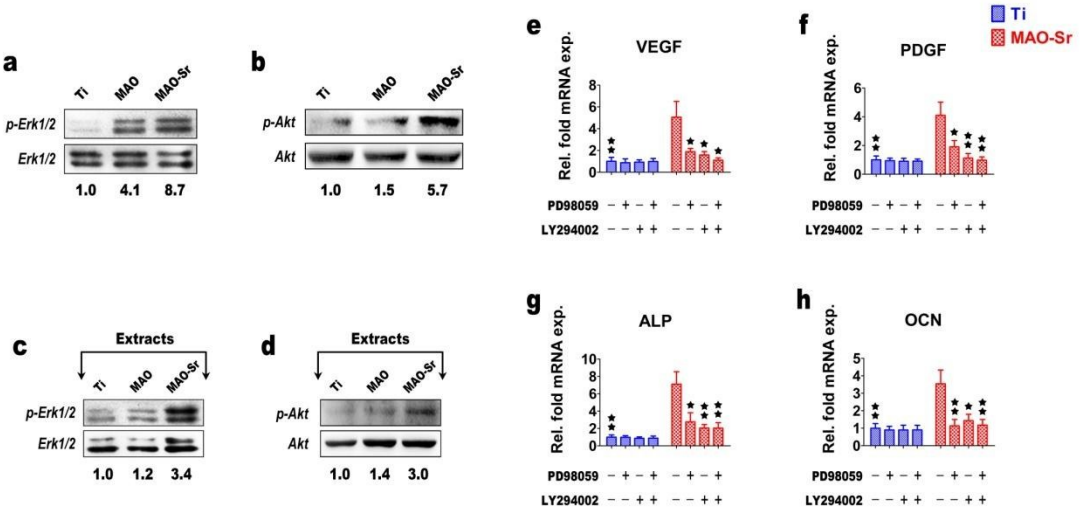

Fig. 6. The mechanisms of the angiogenic/osteogenic effects of the new coatings on canine BMSCs. (a-b) Western blot analysis showed the activation of Erk1/2 and Akt signaling pathways in canine BMSCs incubating on the titanium plates for 12 hours. (c-d) The activation of Erk1/2 and Akt signaling pathways in canine BMSCs was induced by the extracts from different coatings. (e-h) The expression of VEGF, PDGF-BB, ALP, and OCN genes in canine BMSCs incubating on the titanium plates for 3 days with or without specific signaling inhibitors. Error bars represent SD

(n=3). (★, represents $p < 0.05$; ★★, represents $p < 0.01$).

New coatings promote rapid osseointegration

Large animal experiments were further adopted to evaluate the effect of these new coatings on promoting rapid osseointegration. Firstly, the titanium rods were inserted into canine femur bone marrow cavity, containing abundant BMSCs, so we can test the osteoinduction capacity of these coatings on stem cells *in vivo*. X-ray images were taken after six weeks implantation (Fig. S3b, Supporting Information), obvious newly formed bones were found around the implants with the new coatings in the cavity. From the histological images (Fig. S3c-e, Supporting Information), more dense new bones close by the implants were observed in MAO-Sr group, and both of new bone area and the percentage of bone implant contact (BIC) of the MAO-Sr group were significantly higher than the other two groups. These results strongly demonstrated that the new coating containing strontium ions possessed potent osteoinductive ability *in vivo*.

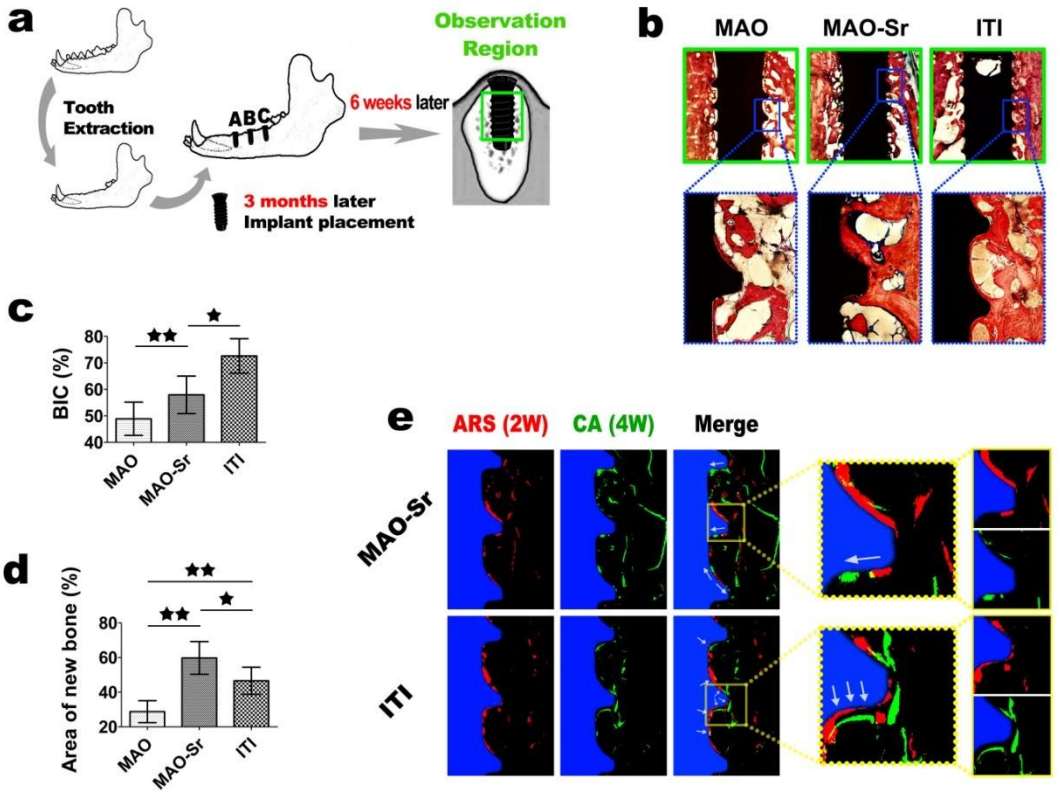

Fig. 7. New coatings promoted rapid osseointegration in canine mandible. (a) Schematic view of

the experimental protocol for the dental implantation surgery. The green rectangular area, including all of the threads, indicated the histological observation region. (b) Histological sections stained with Van Gieson's picro fuchsin solution. (c-d) The statistical results of the percent of BIC and the area of newly-formed bones around the implants. (e) Sequential fluorescent labeling observations. White arrows indicated the main directions of new bone growth. Error bars represent SD (n=3). (★, represents $p < 0.05$; ★★, represents $p < 0.01$).

Then, the new coatings were applied to titanium dental implants, which were screwed in canine mandibles to test the early osseointegration at 6 weeks (Fig. 7a), and the commercially available ITI implants (Straumann AG) were taken as the positive control. Histological images (Fig. 7b) showed new bones adhere closely to the MAO technique processed implant surface, which demonstrated the good biocompatibility of these coatings. In addition, more and robust bones grew around the implant surface containing strontium ions. As we known, the percentage of BIC and the quantity of peri-implant bone area are two vital factors contributing to the quality of osseointegration. Both of the BIC (Fig. 7c) and the area of new bone (Fig. 7d) in the MAO-Sr group were significant higher than that of MAO group. Although the BIC was less when compared to the ITI group, the percent of BIC already reached as high as about 60% and peri-implant new bone area was significantly higher in the MAO-Sr group. Taking all of these results together, the MAO-Sr coating has driven the osseointegration to a high level, which is close to the effect of ITI implants. Interestingly, sequential fluorescent labeling results (Fig. 7e) from week 2 to week 4 indicated that new bones grew outward from the implant surface in the ITI group, but the newly formed bones extended along the surface in the MAO-Sr group. Therefore, the percent of BIC in the MAO-Sr group would be further increased over time, six weeks later. In addition, the released strontium ions *in vivo* might also play a remote action that inducing angiogenesis and osteogenesis in the gap between implant surface and host bones (Fig. 8), to promote rapid new bone formation which could be supported by the more active mineralization around the implants in the MAO-Sr group at both observation time points (Fig. 7e).

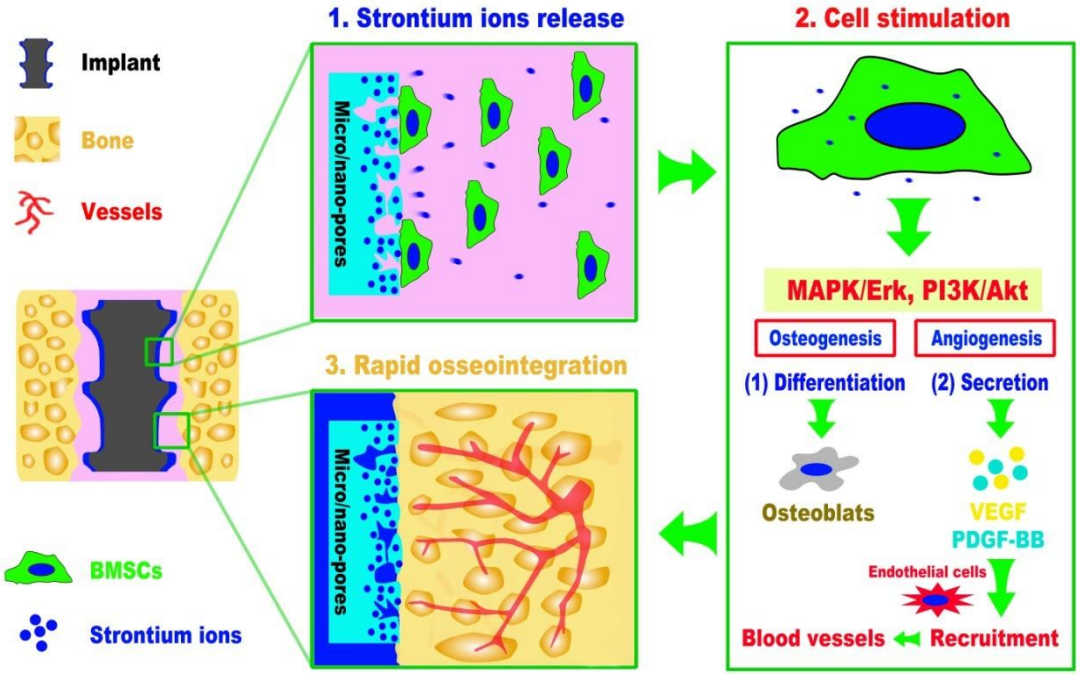

Fig. 8. A general schematic view of the mechanisms of the MAO-Sr coating on promoting rapid integration by facilitating angiogenesis and osteogenesis activities.

Conclusion

Multi-functional titanium implant coatings were fabricated by a new micro-arc oxidation technique for dental implant application. The nanoporous structure not only directly promoted cells adhesion and differentiation, but also could deliver growth factors to enhance its biofunctionalization. Moreover, after strontium ions incorporation, MAO-Sr coating showed obvious angiogenic and osteogenic effects on canine BMSCs via MAPK/Erk and PI3K/Akt signaling pathways. In details, the MAO-Sr coating facilitated their osteogenic differentiation and promoted angiogenic growth factors secretion to recruit endothelial cells and form blood vessels. On the large animal implantation models, the MAO-Sr coating significantly enhanced fast bone formation within initial six weeks. The *in vivo* performance of the MAO-Sr coated dental implants on rapid osseointegration was comparable to that of commercially available ITI implants. These results therefore suggest a novel implant coating to achieve rapid osseointegration by enhancing both of angiogenesis

and osteogenesis.

Acknowledgments

This work was supported in part by the National Basic Research Program of China (973 Program, 2012CB933604), the National Science Fund for Distinguished Young Scholars of China (No.81225006), the National Natural Science Foundation of China (No.81430012), Ph.D innovation fund from Shanghai Jiao Tong University School of Medicine (BXJ201331), Shanghai Rising-Star Program (15QA1404100), and Youth Innovation Promotion Association CAS (2015204). Dr. Jiang would like to acknowledge the Chang Jiang Scholars Programme of the Ministry of Education of China.

References

1. P.-I. Brånemark, U. Breine, R. Adell, B. Hansson, J. Lindström and Å. Ohlsson, *Scandinavian Journal of Plastic and Reconstructive Surgery and Hand Surgery*, 1969, **3**, 81-100.
2. T. Albrektsson, G. Zarb, P. Worthington and A. Eriksson, *Int J Oral Maxillofac Implants*, 1986, **1**, 11-25.
3. L. Le Guéhennec, A. Soueidan, P. Layrolle and Y. Amouriq, *Dental materials*, 2007, **23**, 844-854.
4. C. Wan, S. R. Gilbert, Y. Wang, X. Cao, X. Shen, G. Ramaswamy, K. A. Jacobsen, Z. S. Alaql, A. W. Eberhardt and L. C. Gerstenfeld, *Proceedings of the National Academy of Sciences*, 2008, **105**, 686.
5. J. M. Kanczler and R. O. Oreffo, *Eur Cell Mater*, 2008, **15**, 100-114.
6. A. P. Kusumbe, S. K. Ramasamy and R. H. Adams, *Nature*, 2014, **507**, 323-328.
7. S. K. Ramasamy, A. P. Kusumbe, L. Wang and R. H. Adams, *Nature*, 2014, **507**, 376-380.
8. D. L. Hutton and W. L. Grayson, *Current Opinion in Chemical Engineering*, 2014, **3**, 75-82.
9. L. H. Nguyen, N. Annabi, M. Nikkhah, H. Bae, L. Binan, S. Park, Y. Kang, Y. Yang and A. Khademhosseini, *Tissue Engineering Part B: Reviews*, 2012.
10. W. Zhang, X. Wang, S. Wang, J. Zhao, L. Xu, C. Zhu, D. Zeng, J. Chen, Z. Zhang, D. L. Kaplan and X. Jiang, *Biomaterials*, 2011, **32**, 9415-9424.
11. W. Zhang, C. Zhu, Y. Wu, D. Ye, S. Wang, D. Zou, X. Zhang, D. Kaplan and X. Jiang, *European cells & materials*, 2014, **27**, 1-12.
12. D. Zou, Z. Zhang, D. Ye, A. Tang, L. Deng, W. Han, J. Zhao, S. Wang, W. Zhang, C. Zhu, J. Zhou, J. He, Y. Wang, F. Xu, Y. Huang and X. Jiang, *Stem Cells*, 2011, **29**, 1380-1390.
13. A. Scarano, V. Perrotti, L. Artese, M. Degidi, D. Degidi, A. Piattelli and G. Iezzi, *Odontology*, 2013, 1-8.
14. K. Ito, Y. Yamada, T. Naiki and M. Ueda, *Clinical Oral Implants Research*, 2006, **17**, 579-586.
15. S. E. Lynch, D. Buser, R. A. Hernandez, H. Weber, H. Stich, C. H. Fox and R. C. Williams, *Journal of periodontology*, 1991, **62**, 710-716.
16. W. Zhang, Z. Li, Y. Liu, D. Ye, J. Li, L. Xu, B. Wei, X. Zhang, X. Liu and X. Jiang, *International Journal of Nanomedicine*, 2012, **7**, 4459-4472.
17. X. Liu, P. K. Chu and C. Ding, *Materials Science and Engineering: R: Reports*, 2010, **70**, 275-302.
18. W. Zhang, G. Wang, Y. Liu, X. Zhao, D. Zou, C. Zhu, Y. Jin, Q. Huang, J. Sun, X. Liu, X. Jiang and H. Zreiqat, *Biomaterials*, 2013, **34**, 3184-3195.
19. Y. Qiao, W. Zhang, P. Tian, F. Meng, H. Zhu, X. Jiang, X. Liu and P. K. Chu, *Biomaterials*, 2014, **35**, 6882-6897.
20. W. Zhang, Y. Jin, S. Qian, J. Li, Q. Chang, D. Ye, H. Pan, M. Zhang, H. Cao, X. Liu and X. Jiang, *Nanomedicine: Nanotechnology, Biology and Medicine*, 2014, **10**, 1809-1818.
21. Y. Liu, L. Enggist, A. F. Kuffer, D. Buser and E. B. Hunziker, *Biomaterials*, 2007, **28**, 2677-2686.
22. C. N. Elias and L. Meirelles, *Expert Rev Med Devices*, 2010, **7**, 241-256.
23. W. Zhang, Z. Li, Q. Huang, L. Xu, J. Li, Y. Jin, G. Wang, X. Liu and X. Jiang, *International Journal of Nanomedicine*, 2013, **8**, 257-265.
24. B. Hu, W. Shi, Y. L. Wu, W. R. Leow, P. Cai, S. Li and X. Chen, *Advanced Materials*, 2014, **26**,

5786-5793.

25. A. L. Raines, R. Olivares-Navarrete, M. Wieland, D. L. Cochran, Z. Schwartz and B. D. Boyan, *Biomaterials*, 2010, **31**, 4909-4917.
26. N. Donos, S. Hamlet, N. Lang, G. Salvi, G. Huynh‐Ba, D. Bosshardt and S. Ivanovski, *Clinical Oral Implants Research*, 2011, **22**, 365-372.
27. J. Li, W. Zhang, Y. Qiao, H. Zhu, X. Jiang, X. Liu and C. Ding, *Journal of Materials Chemistry B*, 2014, **2**, 283-294.
28. X. Wang, Y. Wang, L. Li, Z. Gu, H. Xie and X. Yu, *Ceramics International*, 2014, **40**, 6999-7005.
29. Z. Gu, X. Zhang, L. Li, Q. Wang, X. Yu and T. Feng, *Materials Science and Engineering: C*, 2013, **33**, 274-281.
30. F. Liu, X. Zhang, X. Yu, Y. Xu, T. Feng and D. Ren, *Journal of Materials Science: Materials in Medicine*, 2011, **22**, 683-692.
31. C. K. Poh, Z. Shi, T. Y. Lim, K. G. Neoh and W. Wang, *Biomaterials*, 2010, **31**, 1578-1585.
32. E. De Giglio, S. Cometa, M. A. Ricci, A. Zizzi, D. Cafagna, S. Manzotti, L. Sabbatini and M. Mattioli-Belmonte, *Acta Biomaterialia*, 2010, **6**, 282-290.
33. K. C. Popat, M. Eltgroth, T. J. LaTempa, C. A. Grimes and T. A. Desai, *Small*, 2007, **3**, 1878-1881.
34. P. M. Sinha, G. Valco, S. Sharma, X. Liu and M. Ferrari, *Nanotechnology*, 2004, **15**, S585.
35. S. Oh, K. S. Brammer, Y. S. J. Li, D. Teng, A. J. Engler, S. Chien and S. Jin, *Proceedings of the National Academy of Sciences*, 2009, **106**, 2130-2135.
36. Z. Hamidouche, O. Fromigué, J. Ringe, T. Häupl, P. Vaudin, J.-C. Pagès, S. Srouji, E. Livne and P. J. Marie, *Proceedings of the National Academy of Sciences*, 2009, **106**, 18587-18591.
37. A. Manohar, S. G. Shome, J. Lamar, L. Stirling, V. Iyer, K. Pumiglia and C. M. DiPersio, *Journal of Cell Science*, 2004, **117**, 4043-4054.
38. D. D. Schlaepfer, C. R. Hauck and D. J. Sieg, *Progress in biophysics and molecular biology*, 1999, **71**, 435-478.
39. L. E. Benjamin, I. Hemo and E. Keshet, *Development*, 1998, **125**, 1591-1598.
40. P. Carmeliet, *Nature*, 2005, **438**, 932-936.
41. C. Wang, K. Lin, J. Chang and J. Sun, *Biomaterials*, 2013, **34**, 64-77.
42. F.-S. Wang, C.-J. Wang, Y.-J. Chen, P.-R. Chang, Y.-T. Huang, Y.-C. Sun, H.-C. Huang, Y.-J. Yang and K. D. Yang, *Journal of Biological Chemistry*, 2004, **279**, 10331-10337.
43. C. Wan, S. R. Gilbert, Y. Wang, X. Cao, X. Shen, G. Ramaswamy, K. A. Jacobsen, Z. S. Alaql, A. W. Eberhardt, L. C. Gerstenfeld, T. A. Einhorn, L. Deng and T. L. Clemens, *Proc Natl Acad Sci U S A*, 2008, **105**, 686-691.
44. Y. Zhou, X. Guan, M. Yu, X. Wang, W. Zhu, C. Wang, M. Yu and H. Wang, *Biotechnology Journal*, 2014, **9**, 944-953.
45. H. Xie, Z. Cui, L. Wang, Z. Xia, Y. Hu, L. Xian, C. Li, L. Xie, J. Crane and M. Wan, *Nature medicine*, 2014.